Indian Journal of Pure & Applied Physics
Vol. 61, October 2023, pp. 830-839
DOI: 10.56042/ijpap.v61i10.3592

# Unsteady MHD CNTs-blood Nanofluid Flow and Heat Transfer under the Effects of Viscous Dissipation, Resistive heating, and Thermal Radiation over a Sensor Surface Accompanied by Variable Viscosity

Santosh Chaudhary* & Ajay Singh
Department of Mathematics, Malaviya National Institute of Technology, Jaipur, Rajasthan 302 017, India

*Received 4 July 2023; accepted 31 July 2023*

The numerical scrutiny of unsteady incompressible magneto-hydrodynamics (MHD) for blood flow in carbon nano tubes (CNTs), past a sensor surface has been presented under the influences of viscous dissipation, resistive heating, and thermal radiation. The variables without having dimensions have been deployed to alter the reigning flow equations, which are non-linear, coupled partial differential equations (PDEs), into the system of non-linear coupled ordinary differential equations (ODEs). The bvp4c tool of MATLAB software has been exercised to obtain the numerical solutions of the dimensionless governing system. The graphs and tables have been formed for the SWCNT-blood and MWCNT-blood nano-liquids for the velocity and temperature profiles versus the unsteadiness parameter, magnetic parameter, magnetic field inclination angle, radiation parameter, and Eckert number. It has been observed that the velocity profile of MWCNT-blood nanofluid is higher than the velocity profile of SWCNT-blood nanofluid except for radiation parameter and Eckert number. However, a reverse trend has been noted for temperature profiles for both nanofluids for all other governing parameters. The comparison tables, for the values of the local skin friction factor and the local Nusselt number, for the various governing parameters, match with outcomes of the previously reported data and validate the employed technique for the solution.

**Keywords:** MHD; Nanofluid; Viscous dissipation; Resistive heating; Thermal radiation; Sensor surface

## 1 Introduction

In Magneto-hydrodynamics (MHD) fluid dynamics studies the electrically conducting substances have been extensively analyzed under the effect of magnetism. The characteristics of the magnetic field, like the strength to alter the flow field[1] and the reliable process to rein the momentum and heat movement of the flow field[2], have made it an appealing topic for research. Its vast range of applications in sundry fields of technology and industries as chemical and fuel industries, formation of crystals, metallurgical operations, MHD pipe flows, cancer therapy, plasma studies, astronomy, *etc*., justify its significant demand and interest among researchers and scientists[3,4,5]. Initially, the movement of electrically conductive liquid in the impedance of magnetic effect was pioneered by Hartmann[6], which further led to the extensive investigation of MHD. Tian *et al.*[7] have illustrated a numerical analysis of a convective unsteady MHD nano-liquid flow and found that the dispersed nanoparticles lead to an enhancement in the heat transfer while noticing the significant enervate in the fluid flow. Further, the MHD flow of nano-liquid, taking into consideration the dissipation, resistive heating, and Newtonian heating, was examined by Chaudhary and Kanika[8]. After that, the unsteady MHD movement of Powell-Eyring nano-liquid has been conferred by Patil *et al.*[9]. Doley *et al.*[10] examined the MHD time fractional transient flow of hybrid nanofluid with an applied magnetic field and viscous dissipation past impulsively started vertical plate using the finite difference method. Recently, Alsaedi *et al.*[11] has bestowed the numerical scrutiny of the MHD hybrid nanoliquid flow between two cylinders that shares the same axis.

Nowadays, a noteworthy advancement in nanotechnology has made nanofluids a cynosure among various fields. A considerable curiosity in the study and research of nanofluids by scientists, engineers, industrialists, and other people and a long series of applications of nanofluids in several fields of science and technology justify the word 'cynosure'. Electronic chip cooling, paintings, atomic reactors, ceramics, medical purposes, jets, solar collectors, crystal growth, and material synthesis has been on the long list of its usage[12,13,14]. Heat transport capability and high thermal capacity distinguish nanofluids from

*Corresponding author: (E-mail: d11.santosh@yahoo.com)

traditional base fluids due to the particle size and surface area. An amalgam of the base fluid and nano-sized particles has been termed as the word 'nanofluid', which was designated by Choi and Eastman[15]. Krishna and Chamkha[16] have explored the impacts of Hall and Ion-slip on an MHD nanofluid flow over an infinite vertical plate. They found that corresponding booming values of radiation parameter lead to an increment in the thermal boundary layer thickness. A comparative study between hybrid nanofluid and nanofluid near the stagnation point for an MHD flow was described by Aly and Pop[17]. Recently, Chaudhary *et al.*[18] and Maiti *et al.*[19] discussed the MHD nanofluid flow with specified conditions.

When traveling, fluid has to work on adjacent flow layers due to the fluid's viscosity. Consequently, the kinetic energy of a fluid's flow transmutes into heat; this process has been termed 'viscous dissipation'. On the contrary, heat arises when the electrically conductive fluid travels through the magnetic field, and this phenomenon is named 'Joule' or 'Ohmic' heating. Maynes and Webb[20] have presented the influences of viscous dissipation on a completely evolved electro-osmotic heat transfer in microchannels. They concluded that the influences of viscous dissipation are crucial only at inferior values of the comparative duct radius. After that, the numerical investigation of an unsteady stagnation point flow considering the effects of viscous dissipation and resistive heating had been analyzed by Chaudhary and Kanika[21]. Gholinia *et al.*[22] scrutinized Walters-B nanofluid's free convection MHD flow while considering the Joule heating impacts. A numerical study of the influences of friction drag, resistive heating, and viscous dissipation was unmasked by Khan *et al.*[23], resulting in friction drag growing along with the increment in slip velocity. Currently, Doley *et al.*[24] studied the heat transfer between moving material and ambient medium past an impulsively started vertical plate along with viscous dissipation, thermal radiation, and applied magnetic field.

Thermal radiation represents the energy continuously emanating from all objects due to temperature disparity. Thermal radiation has applications in elevated temperature and designing procedures like propulsion tools for space carriage and aircraft, nuclear power plants, solar technology, thermonuclear fusion, polymer processing, furnaces, and fires, among others[25,26]. Siddheshwar and Mahabaleswar[27] analyzed the impacts of radiation on the MHD flow of a viscoelastic liquid. After that, the MHD nano-liquid flow, along with the chemical reaction, was explored by Daniel *et al.*[28], and along with Marangoni convection, was explained by Chaudhary and Kanika[29]. Sedki *et al.*[30] have presented the radiation impact on an unsteady mixed convective movement and heat transfer of nano-liquid upon a stretchable surface. Recently, Priyadharsini and David[31] explored the effect of thermal radiation and an applied magnetic field on stretching and permeable blood capillary along with thermoregulation on blood viscosity.

As per the author's best knowledge, the effect of magnetic field inclination angle, viscous dissipation, resistive heating, and radiation impact on MHD unsteady flow of CNTs-blood nano-liquids over a sensor sheet with variable viscosity have not been investigated yet. Specifically, the variable viscosity has been assumed. The velocity, temperature profiles, local skin friction factor, and local Nusselt number have been studied and reviewed for the various values of controlling parameters for both SWCNT-blood and MWCNT-blood nano-liquids. The solutions of governing equations obtained by computational technique, namely, bvp4c of software MATLAB, and outcomes of these equations have been verified via comparative tables.

## 2 Physical Replica and Formulation of the Problem

An unsteady, incompressible, two-dimensional, electrically conductive CNTs-blood nano-liquid flow past a sensor sheet has been considered. In this model it has been taken that the nano-liquid flow passes through two endless parallel plates, installed in such a way that the surface of the problem is confined within a compressing channel with width $h(t)$. Additionally, the upper plate gets compressed while keeping the lower plate fixed. A viscosity sensor with length $l$, among the types of micro-cantilever sensors, is established between analogous plates. The temperature-dependent viscosity of a fluid has been assumed. The assumed problem's physical replica can be seen in Fig. 1, where $x-$axis represents the flow direction, and the $y-$ axis is normal to it. $u$, and $v$ are signifying the velocity components along $x$, and $y$ directions, respectively. A slanting magnetic field $B_{mf}$ with acute angle $\delta$ is enforced in the direction of

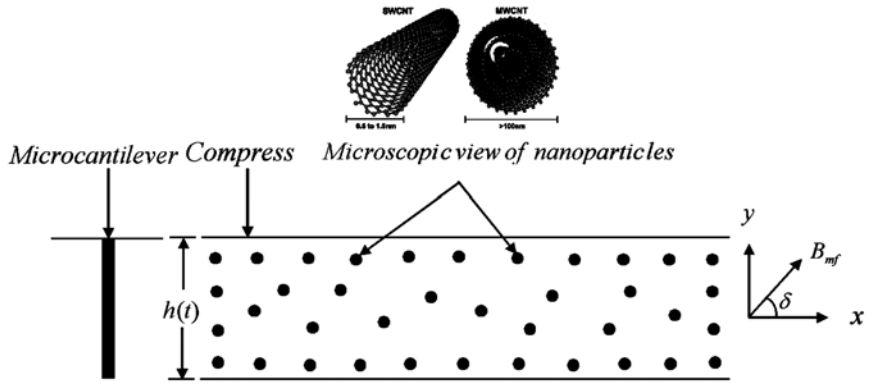


Fig. 1 — Schematic model

$x-$axis. $T_w$ and $T_{am}$ are used to signify the surface and ambient temperature, respectively, where $T_w < T_{am}$. According to stated assumptions, the governing equations of the present work can be expressed as[32]

$$\frac{\partial u}{\partial x}+\frac{\partial v}{\partial y}=0 \qquad \ldots (1)$$

$$\rho_{nf}\left(\frac{\partial u}{\partial t}+u\frac{\partial u}{\partial x}+v\frac{\partial u}{\partial y}\right)=\rho_{nf}\left(\frac{\partial U_{ex}}{\partial t}+U_{ex}\frac{\partial U_{ex}}{\partial x}\right)+\frac{\partial}{\partial y}\left(\mu_{nf}(T)\frac{\partial u}{\partial y}\right)+(\sigma_{ec})_{nf}B_{mf}^2\sin^2(\delta)(U_{ex}-u) \qquad \ldots (2)$$

$$(\rho C_p)_{nf}\left(\frac{\partial T}{\partial t}+u\frac{\partial T}{\partial x}+v\frac{\partial T}{\partial y}\right)=\kappa_{nf}\frac{\partial^2 T}{\partial y^2}+\mu_{nf}(T)\left(\frac{\partial u}{\partial y}\right)^2-\frac{\partial q_R}{\partial y}+(\sigma_{ec})_{nf}B_{mf}^2\sin^2(\delta)(U_{ex}-u)^2 \qquad \ldots (3)$$

subject to the boundary restrictions

$$y=0 \;:\; u=0,\quad v=\sqrt{\frac{\nu_{ff}}{(q+rt)}}k_0,\quad T=T_w(x,t) \qquad \ldots (4)$$
$$y\to\infty:\; u\to U_{ex},\quad T\to T_{am}$$

Subscripts $nf$ and $ff$ stand for the nanofluid and fundamental fluid, respectively. Notations $t$, $q$, $r$, and $k_0$ represent the time, positive constant, unsteadiness parameter, and permeable velocity parameter. Notations $\rho$, $\mu$, $\sigma_{ec}$, $\rho C_p$, $T$, $\kappa$, and $\nu$ are for the density, dynamic viscosity, electrical conductivity, heat capacitance, temperature, thermal conductivity, and kinematic viscosity of the fluid, respectively. External flow velocity $U_{ex}=\frac{x}{q+rt}$, surface temperature $T_w(x,t)=T_{am}+T_0\frac{rx}{(q+rt)^{-1/2}}$, where $T_0$ is the reference temperature.

Radiative heat flux[33] can be inscribed as

$$q_R=-\frac{4\sigma_{sb}}{3k_{rm}}\frac{\partial T^4}{\partial y} \qquad \ldots (5)$$

$\sigma_{sb}$ and $k_{rm}$ allude to the Stefan-Boltzmann constant and, Rosseland mean absorption factor, respectively.

After employing Taylor's series approximation of $T^4$ around ambient temperature $T_{am}$ in equation (5),

$$\frac{\partial q_R}{\partial y}=-\frac{16\sigma_{sb}T_{am}^3}{3k_{rm}}\frac{\partial^2 T}{\partial y^2} \qquad \ldots (6)$$

The thermophysical characteristics of $CNTs-$blood nano-liquid can be manifested as follows[29,32]

$$\frac{\rho_{nf}}{\rho_{ff}}=(1-\varphi)+\varphi\frac{\rho_{cnt}}{\rho_{ff}},\quad \frac{\mu_{nf}(T)}{\mu_{ff}(T)}=\frac{1}{(1-\varphi)^{5/2}},$$
$$\frac{(\sigma_{ec})_{nf}}{(\sigma_{ec})_{ff}}=1+\frac{3\left[\frac{(\sigma_{ec})_{cnt}}{(\sigma_{ec})_{ff}}-1\right]\varphi}{2+\frac{(\sigma_{ec})_{cnt}}{(\sigma_{ec})_{ff}}-\left[\frac{(\sigma_{ec})_{cnt}}{(\sigma_{ec})_{ff}}-1\right]\varphi}, \qquad \ldots (7)$$
$$\frac{(\rho C_p)_{nf}}{(\rho C_p)_{ff}}=(1-\varphi)+\varphi\frac{(\rho C_p)_{cnt}}{(\rho C_p)_{ff}},$$
$$\frac{\kappa_{nf}}{\kappa_{ff}}=\frac{(1-\varphi)+2\frac{\kappa_{cnt}}{\kappa_{cnt}-\kappa_{ff}}\ln\frac{\kappa_{cnt}+\kappa_{ff}}{2\kappa_{ff}}\varphi}{(1-\varphi)+2\frac{\kappa_{ff}}{\kappa_{cnt}-\kappa_{ff}}\ln\frac{\kappa_{cnt}+\kappa_{ff}}{2\kappa_{ff}}\varphi}$$

Where $\varphi$ and subscript $cnt$ allude to the volume fraction parameter and carbon nano-tubes, respectively.

## 3 Transformation Technique

The following non-dimensional similarity variables have been utilized to obtain a system of coupled ODEs

$$\psi(x,y,t)=\sqrt{\frac{\nu_{ff}}{(q+rt)}}\,x f(\eta),\quad \eta=\sqrt{\frac{1}{(q+rt)\nu_{ff}}}\,y,\quad \theta(\eta)=\left(\frac{T-T_{am}}{T_w-T_{am}}\right)$$
$$u=\frac{\partial\psi}{\partial y},\quad v=-\frac{\partial\psi}{\partial x} \qquad \ldots (8)$$

Where $\psi$, $\eta$, $f$, and $\theta$ signify the stream function, similarity variable, non-dimensional velocity, and temperature, respectively.

Temperature dependant dynamic viscosity is defined as

$$\mu_{ff}(\theta)=\mu_{ff}e^{-\beta\theta}\cong 1-\beta\theta+O(\beta^2) \qquad \ldots (9)$$

Now, by employing equations (5) - (9) into equations (1) - (4), the transmuted flow reigning equations and boundary restrictions are

$$\frac{e^{-\beta\theta}}{(1-\varphi)^{5/2}}(f'''-\beta f'')+\left[(1-\varphi)+\varphi\frac{\rho_{cnt}}{\rho_{ff}}\right]\left[\left(f+\frac{r}{2}\eta\right)f''-f'^2+r(f'-1)+1\right]+\frac{(\sigma_{ec})_{nf}}{(\sigma_{ec})_{ff}}M\sin^2(\delta)(1-f')=0 \qquad \ldots (10)$$

$$\frac{\left(\frac{\kappa_{nf}}{\kappa_{ff}}+R\right)}{\Pr}\theta''+\left[(1-\varphi)+\varphi\frac{(\rho C_p)_{cnt}}{(\rho C_p)_{ff}}\right]\left[f\theta'-f'\theta+\frac{r}{2}(\eta\theta'-\theta)\right]+\frac{e^{-\beta\theta}}{(1-\varphi)^{5/2}}Ecf''^2+\frac{(\sigma_{ec})_{nf}}{(\sigma_{ec})_{ff}}M\sin^2(\delta)Ec(1-f')^2=0 \qquad \ldots (11)$$

$$f=-k_0,\quad f'=0,\quad \theta=1\quad at\quad \eta=0$$
$$f'\to 1,\quad \theta\to 0\quad as\quad \eta\to\infty \qquad \ldots (12)$$

Here,

$$\beta,\ M=\frac{(q+rt)(\sigma_{ec})_{ff}B_{mf}^2}{\rho_{ff}},\ \Pr=\frac{(\mu C_p)_{ff}}{\kappa_{ff}},\ R=\frac{16\sigma_{sb}T_{am}^3}{3k_{rm}\kappa_{ff}},\ Ec=\frac{U_{ex}^2}{(C_p)_{ff}(T_w-T_{am})}$$

allude the dimensionless viscosity parameter, magnetic parameter, Prandt l number, radiation parameter, and Eckert number, respectively.

The prominent engineering quantities of interest for the flow are the local skin friction factor $C_{sfx}$ and local Nusselt number $Nu_{nnx}$. Mathematically, they can be inscribed as follows

$$C_{sfx}=\frac{(q+rt)^2}{x^2}\frac{\mu_{nf}(T)}{\rho_{ff}}\left(\frac{\partial u}{\partial y}\right)_{y=0},$$
$$Nu_{nnx}=-\left(\frac{\kappa_{nf}}{\kappa_{ff}}\right)\frac{x}{(T_w-T_{am})}\left(\frac{\partial T}{\partial y}\right)_{y=0}+\frac{x}{(T_w-T_{am})}\left(\frac{q_R}{\kappa_{ff}}\right)_{y=0} \qquad \ldots (13)$$

Now, employing similarity equation (8) into equation (13), the following equations have been attained

$$\mathrm{Re}_{rx}^{1/2}C_{sfx}=\frac{\left(1-\beta\theta+O(\beta^2)\right)}{(1-\varphi)^{5/2}}f''(0), \qquad \ldots (14)$$
$$\mathrm{Re}_{rx}^{-1/2}Nu_{nnx}=-\left(\frac{\kappa_{nf}}{\kappa_{ff}}+R\right)\theta'(0)$$

Where, local Reynolds number $\mathrm{Re}_{rx}=\frac{1}{(q+rt)}\frac{x^2}{\nu_{ff}}$

## 4 Solution Methodology and Validation

This section explains the modus operandi to solve the dimensionless reigning flow equations (10) – (11) and the boundary restrictions equation (12). The bvp4c tool of the software MATLAB is operated to acquire numerical outcomes. To apply this method, the governing equations have been written into the system of coupled first-order differential equations, then employed the best-suited initial guess and enlisted the solution of the proposed problem. The mechanism for this process has been as under:

Assuming

$$h_1=f,\quad h_2=f',\quad h_3=f'',\quad h_4=\theta,\quad h_5=\theta' \qquad \ldots (15)$$

in the equations (10)-(12), the transformations obtained are:

$$h_3'=-e^{\beta\theta}(1-\varphi)^{5/2}\left[(1-\varphi)+\varphi\frac{\rho_{cnt}}{\rho_{ff}}\right]\left[\left(h_1+\frac{r}{2}\eta\right)h_3-h_2^2+r(h_2-1)+1\right]+\beta h_3-e^{\beta\theta}(1-\varphi)^{5/2}\frac{(\sigma_{ec})_{nf}}{(\sigma_{ec})_{ff}}M\sin^2(\delta)(1-h_2) \qquad \ldots (16)$$

$$h_5'=-\frac{\Pr}{\left(\frac{\kappa_{nf}}{\kappa_{ff}}+R\right)}\left\{\left[(1-\varphi)+\varphi\frac{(\rho C_p)_{cnt}}{(\rho C_p)_{ff}}\right]\left[h_1h_5-h_2h_4+\frac{r}{2}(\eta h_5-h_4)\right]+\frac{e^{-\beta\theta}}{(1-\varphi)^{5/2}}Ech_3^2+\frac{(\sigma_{ec})_{nf}}{(\sigma_{ec})_{ff}}M\sin^2(\delta)Ec(1-h_2)^2\right\} \qquad \ldots (17)$$

and the boundary restrictions are

$$h_1(0)=-k_0,\quad h_2(0)=0,\quad h_4(0)=1$$
$$h_2(\infty)\to 1,\quad h_4(\infty)\to 0 \qquad \ldots (18)$$

Table 1 — Comparative numerical data for local skin friction factor for varied values of $\beta$ and $k_0$ with $r = 1.0,\ M = 0.5$, $\delta = \frac{\pi}{2}$, $\Pr = 6.2$, $R = 0.0$, $Ec = 0.0$

| | Akbar and Khan[32] $\beta = 0.0$ | | Present results $\beta = 0.0$ | | Akbar and Khan[32] $\beta = 0.2$ | | Present results $\beta = 0.2$ | |
|---|---|---|---|---|---|---|---|---|
| $\varphi$ | SWCNT | MWCNT | SWCNT | MWCNT | SWCNT | MWCNT | SWCNT | MWCNT |
| | | | | $k_0 = -0.5$ | | | | |
| 0.0 | 1.38220 | 1.38220 | 1.38220104 | 1.38220104 | 1.35584 | 1.35584 | 1.35584484 | 1.35584484 |
| 0.1 | 1.65680 | 1.57616 | 1.65682580 | 1.57616983 | 1.60355 | 1.52736 | 1.60526531 | 1.52908909 |
| 0.2 | 1.99106 | 1.81981 | 1.99110294 | 1.81984105 | 1.91243 | 1.75107 | 1.91498143 | 1.75364274 |
| | | | | $k_0 = 0.5$ | | | | |
| 0.0 | 0.74805 | 0.74805 | 0.74804830 | 0.74804830 | 0.69905 | 0.69905 | 0.69905277 | 0.69905277 |
| 0.1 | 0.91652 | 0.90160 | 0.91651886 | 0.90160648 | 0.84897 | 0.83790 | 0.84985407 | 0.83879663 |
| 0.2 | 1.14423 | 1.10479 | 1.14423955 | 1.10479873 | 1.05523 | 1.02454 | 1.05676584 | 1.02609100 |

Table 2 — Comparative numerical data for local Nusselt number for varied values of $\beta$ and $k_0$ with $r = 1.0,\ M = 0.5$, $\delta = \frac{\pi}{2}$, $\Pr = 6.2$, $R = 0.0$, $Ec = 0.0$

| | Akbar and Khan[32] $\beta = 0.0$ | | Present results $\beta = 0.0$ | | Akbar and Khan[32] $\beta = 0.2$ | | Present results $\beta = 0.2$ | |
|---|---|---|---|---|---|---|---|---|
| $\varphi$ | SWCNT | MWCNT | SWCNT | MWCNT | SWCNT | MWCNT | SWCNT | MWCNT |
| | | | | $k_0 = -0.5$ | | | | |
| 0.0 | 4.68295 | 4.68295 | 4.68295457 | 4.68295457 | 4.71287 | 4.71287 | 4.71287194 | 4.71287194 |
| 0.1 | 6.32439 | 6.16552 | 6.13758176 | 5.97529637 | 6.39193 | 6.22911 | 6.20153669 | 6.03517706 |
| 0.2 | 7.65429 | 7.37432 | 7.33736912 | 7.05010092 | 7.74869 | 7.46248 | 7.42628970 | 7.13246508 |
| | | | | $k_0 = 0.5$ | | | | |
| 0.0 | 1.18613 | 1.18613 | 1.18613267 | 1.18613267 | 1.21006 | 1.21006 | 1.21006179 | 1.21006179 |
| 0.1 | 2.91731 | 2.76998 | 2.74425078 | 2.59335404 | 2.96951 | 2.82026 | 2.79383182 | 2.64089252 |
| 0.2 | 4.41683 | 4.15591 | 4.11906169 | 3.85006601 | 4.49037 | 4.22674 | 4.18846322 | 3.91644939 |

The initial guesses and mesh points have been chosen so that results obtained are with relative tolerance $10^{-7}$. In the current investigation, $\eta_\infty = 4.0$ has been presumed.

The comparative accuracy of the obtained numerical data with the previously reported data by Akbar and Khan[32], in limited cases, has been presented w.r.t relative values of the local skin friction factor in Table 1 and relative values of the local Nusselt number in Table 2. These tables substantiate the effectiveness of the method employed in this study and further validate the precision of the acquired data.

## 5 Results and discussion

In this section the analysis of velocity and temperature profile graphs has been highlighted along with the tables for SWCNT-blood and MWCNT-blood nanofluids.

$\beta = 0.9, \varphi = 0.3, r = 4.0, M = 5.0, \delta = \pi/2, \Pr = 25.0, R = 2.0, Ec = 0.1, k_0 = 3.0$ are the default values of reigning parameters which have been chosen for the enumeration motive. Table 3 displays the thermo-physical characteristics of the human blood, SWCNT, and MWCNT. The impact of sundry parameters like dimensionless viscosity parameter $\beta$, volume fraction parameter $\varphi$, unsteadiness parameter $r$, the magnetic parameter $M$, magnetic field inclination angle $\delta$, radiation parameter $R$, Eckert number $Ec$, and permeable velocity parameter $k_0$ on the local skin friction factor $C_{sfx}$ and local Nusselt number $Nu_{nnx}$ for the SWCNT-blood and MWCNT-blood nanofluids, while setting $\Pr = 25.0$ have been depicted in Table 4. It is evident from Table 4 that the local skin friction factor

Table 3 — Thermophysical characteristics of employed materials [29, 34]

| Characteristics | Human blood | SWCNT | MWCNT |
|---|---|---|---|
| $\rho(Kg/m^3)$ | 1063 | 2600 | 1600 |
| $\sigma_{ec}(S/m)$ | 0.8 | $10^6$—$10^7$ | $1.9 \times 10^{-4}$ |
| $C_p(J/KgK)$ | 3594 | 425 | 796 |
| $\kappa(W/mK)$ | 0.492 | 6600 | 3000 |

Table 4 — Numerical outcomes of local skin friction factor $C_{sfx}$ and local Nusselt number $Nu_{nnx}$ with setting $\Pr = 25.0$ for SWCNT-blood and MWCNT-blood nanofluids

| | | | | | | | | $C_{sfx}$ | | $Nu_{nnx}$ | |
|---|---|---|---|---|---|---|---|---|---|---|---|
| $\beta$ | $\varphi$ | $r$ | $M$ | $\delta$ | $R$ | $Ec$ | $k_0$ | SWCNT | MWCNT | SWCNT | MWCNT |
| 0.1 | 0.3 | 4.0 | 5.0 | π/2 | 2.0 | 0.1 | 3.0 | 2.70642444 | 3.12220885 | 4.87628196 | 4.32140177 |
| 0.5 | | | | | | | | 1.83643263 | 2.18467521 | 5.19227668 | 4.64282894 |
| 0.9 | | | | | | | | 0.53390699 | 0.71330630 | 5.86933969 | 5.41566968 |
| | 0.1 | | | | | | | 0.15366581 | 0.18362185 | 2.57144576 | 2.48860375 |
| | 0.2 | | | | | | | 0.28528066 | 0.37166369 | 3.97465441 | 3.75866626 |
| | 0.3 | 6.0 | | | | | | 0.43847082 | 0.66746007 | 8.78786849 | 8.16097611 |
| | | 8.0 | | | | | | 0.29742010 | 0.59108627 | 11.60274837 | 10.84744468 |
| | | 4.0 | 2.0 | | | | | 0.04311786 | 0.16862304 | 5.91291025 | 5.62848551 |
| | | | 8.0 | | | | | 0.89986654 | 1.10604246 | 5.585916830 | 5.07137969 |
| | | | 5.0 | π/6 | | | | -0.13725802 | -0.04821849 | 5.62160164 | 5.26808522 |
| | | | | π/3 | | | | 0.35337291 | 0.51597419 | 5.75553415 | 5.34371666 |
| | | | | π/2 | 5.0 | | | 0.53784034 | 0.71926846 | 8.04750602 | 7.63861972 |
| | | | | | 8.0 | | | 0.53997757 | 0.72252038 | 10.24138602 | 9.88873751 |
| | | | | | 2.0 | 0.5 | | 0.45023661 | 0.60243086 | 1.77256497 | 1.30415512 |
| | | | | | | 0.9 | | 0.38460046 | 0.51332994 | -1.79725654 | -2.10539443 |
| | | | | | | 0.1 | 1.0 | 1.59467517 | 1.76209916 | 14.49621269 | 13.60044112 |
| | | | | | | | 2.0 | 0.91399396 | 1.11754654 | 8.98230139 | 8.28340592 |

for the MWCNT-blood has an upper edge relative to SWCNT-blood nanofluid, but the local Nusselt number follows the reverse pattern. The local skin friction factor and local Nusselt number increase corresponding to the rising values of the volume fraction parameter, magnetic field inclination angle, and radiation parameter. However, both display the reduction behavior for the growing values of the Eckert number and permeable velocity parameter. Further, an increment in magnetic parameters causes a advancement in the local skin fraction factor but a reduction in the local Nusselt number. On the contrary, the local skin friction factor reduces while the local Nusselt number enlarges, corresponding to the rising values of the dimensionless viscosity and unsteadiness parameters.

In Figs. 2 & 3 the effect of unsteadiness parameter $r$ on the velocity, and temperature profiles, respectively, for the SWCNT-blood and MWCNT-blood nanofluids has been demonstrated. The velocity and temperature profiles show the behavior of decrement corresponding to the increment in the unsteadiness parameter for both nanofluids. The enlargement of the unsteadiness parameter causes turbulence in the flow or thermal conditions. This increased turbulence can lead to enhanced mixing between fluid or thermal layers, causing a more uniform distribution of velocities and temperatures.

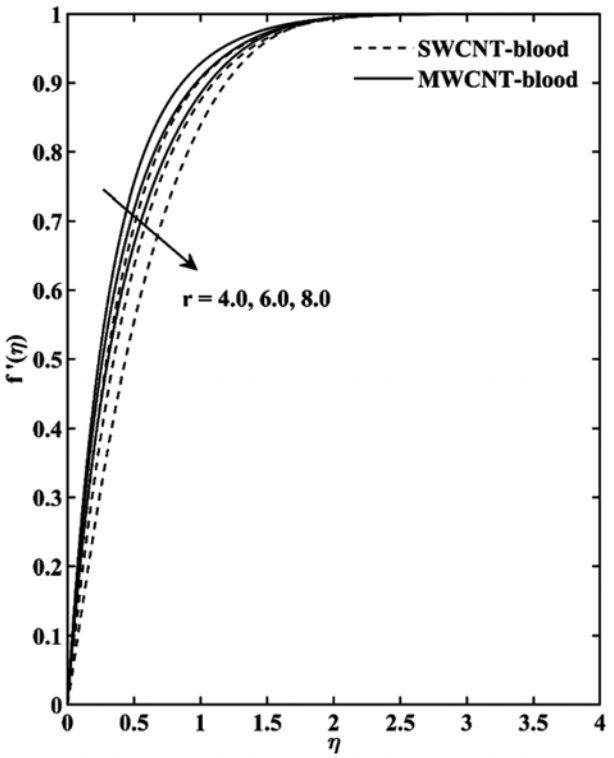


Fig. 2 — Velocity profile for unsteadiness parameter $r$ .

Consequently, the velocity and temperature gradients, which characterize the rate of change, decrease.

The impact of magnetic parameter $M$ , on the velocity and temperature profiles, has been displayed

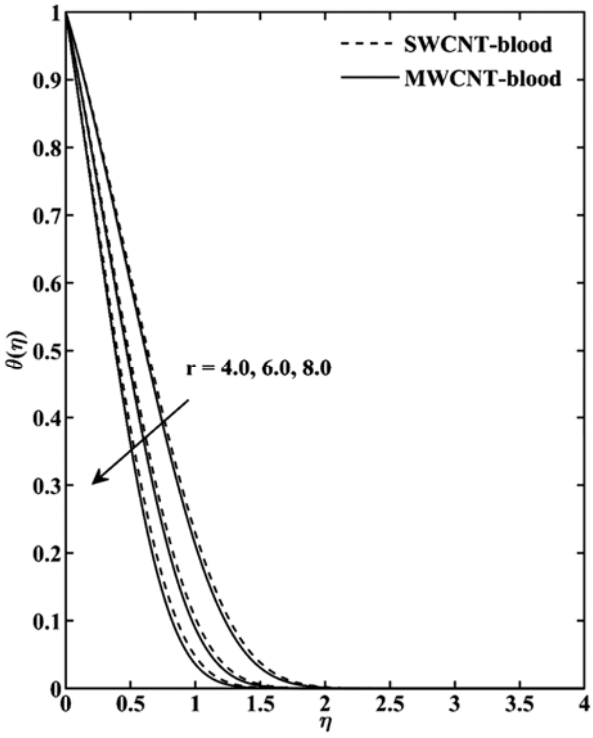


Fig. 3 — Temperature profile for unsteadiness parameter $r$ .

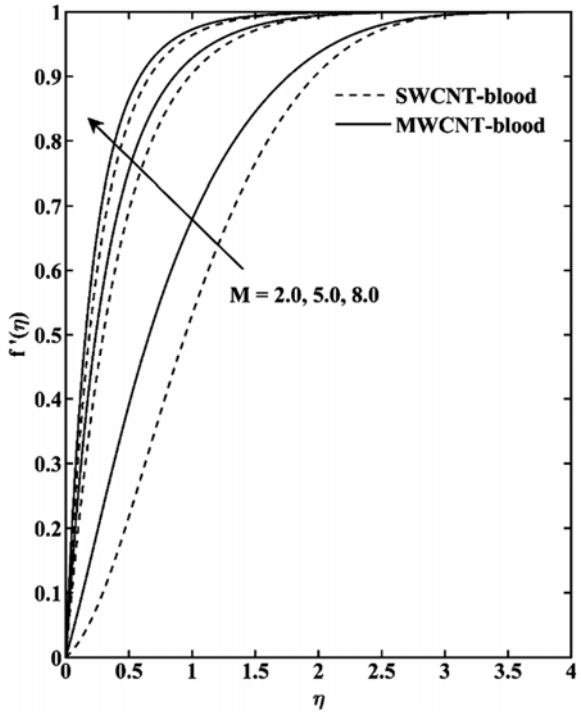


Fig. 4 — Velocity profile for magnetic parameter $M$ .

by the Figs. 4 & 5, respectively, for the SWCNT-blood and MWCNT-blood nanofluids. It has been observed that the velocity profile increases while the

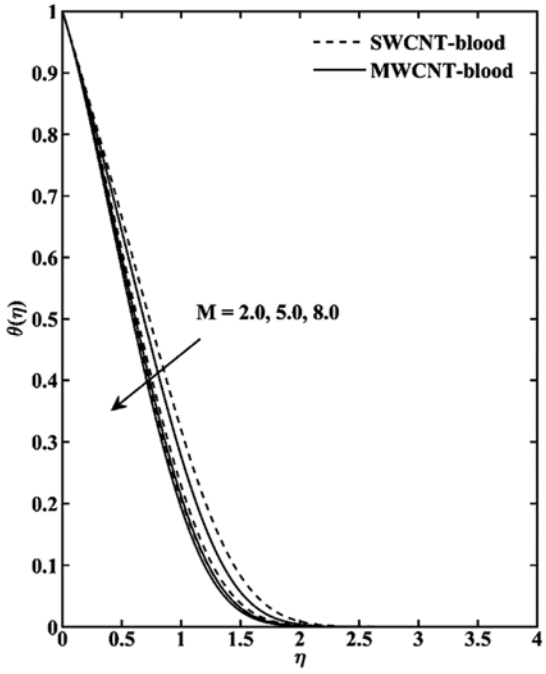


Fig. 5 — Temperature profile for magnetic parameter $M$ .

temperature profile decreases for the growing values of the magnetic parameters for both nanofluids. A rise in the magnetic parameter means an increment in the strength of the magnetic field. Increasing the magnetic field strength can enlarge the Lorentz force, resulting in a more significant influence on the fluid flow. It causes growth in the velocity of the fluid. On the other hand, eddies or vortices are induced by the Lorentz force. Consequently, the heat transfer pattern is altered, and a decrement in temperature distribution is sighted.

In Figs. 6 & 7 the influence of magnetic field inclination angle $\delta$ on the velocity, and temperature distributions, respectively, for the SWCNT-blood and MWCNT-blood nanofluids has been exhibited. The velocity increases while temperature decreases for both nanofluids corresponding to the enhancement in magnetic field inclination angle. An increasing magnetic field inclination angle can cause the fluid velocity to develop because of the degression in the Lorentz force component in the flow direction. Simultaneously, the temperature of the fluid decreases because of the truncated resistive heating associated with the shortened Lorentz force.

The graphs which display the efficacy of radiation parameter $R$ on the velocity and temperature distributions have been sighted in Figs. 8 & 9, respectively, for the SWCNT-blood and MWCNT-

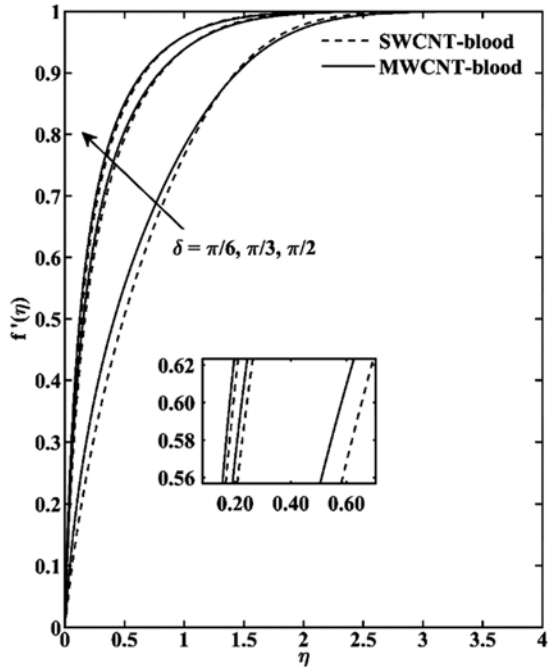


Fig. 6 — Velocity profile for magnetic field inclination angle $\delta$ .

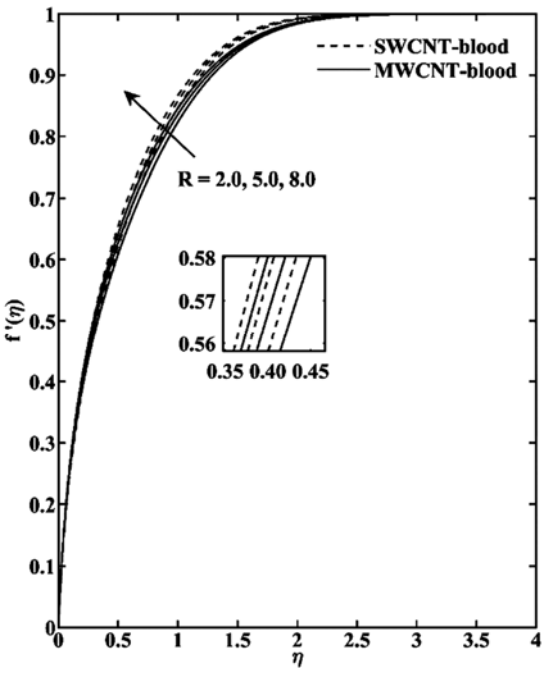


Fig. 8 — Velocity profile for radiation parameter $R$ .

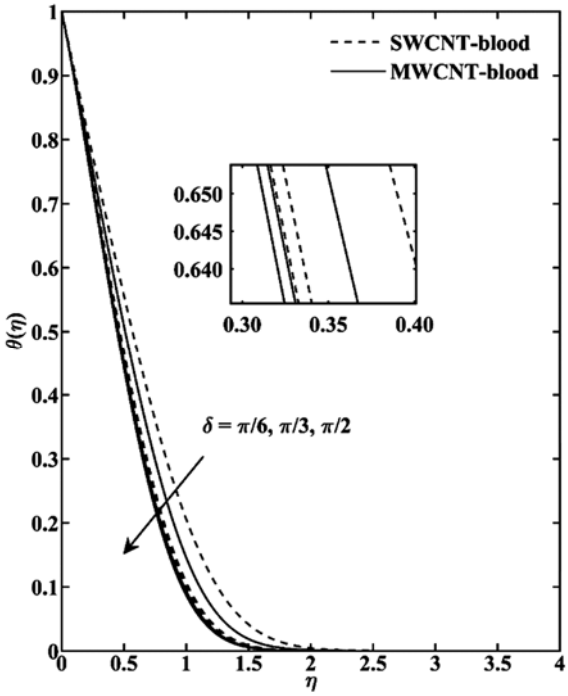


Fig. 7 — Temperature profile for magnetic field inclination angle $\delta$.

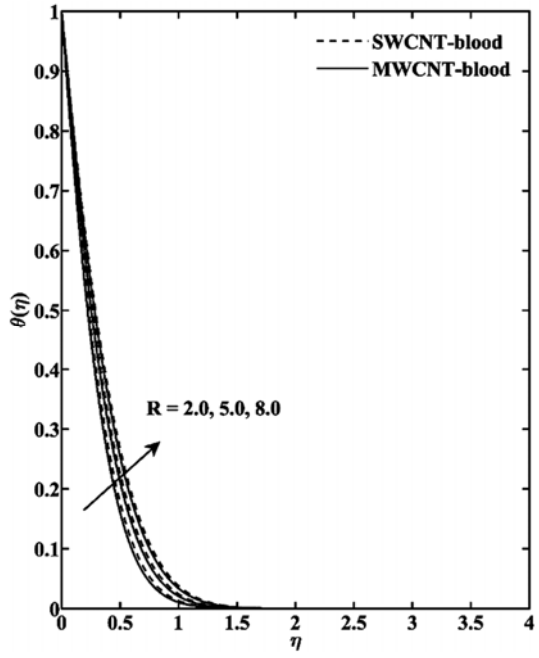


Fig. 9 — Temperature profile for Radiation parameter $R$ .

blood nanofluids. They demonstrate that the velocity and temperature of the fluid enhance when the radiation parameter increases for both nanofluids. As the radiation parameter increases, the fluid absorbs more energy from the incoming radiation; the temperature of the fluid enhances. As the temperature rises, the fluid viscosity decreases, this results in less resistive the fluid, which leads to a rise in the velocity of the fluid.

Figs. 10 & 11 represent the velocity and temperature distributions, respectively, corresponding

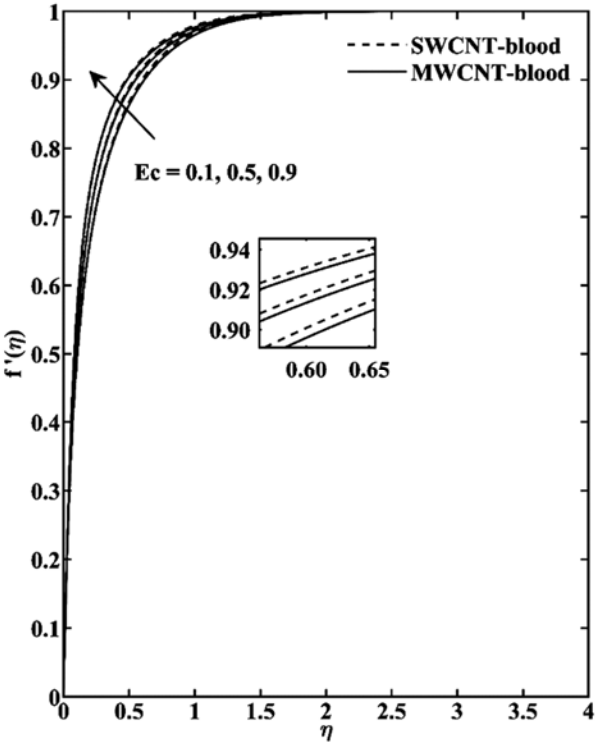


Fig. 10 — Velocity profile for Eckert number $Ec$ .

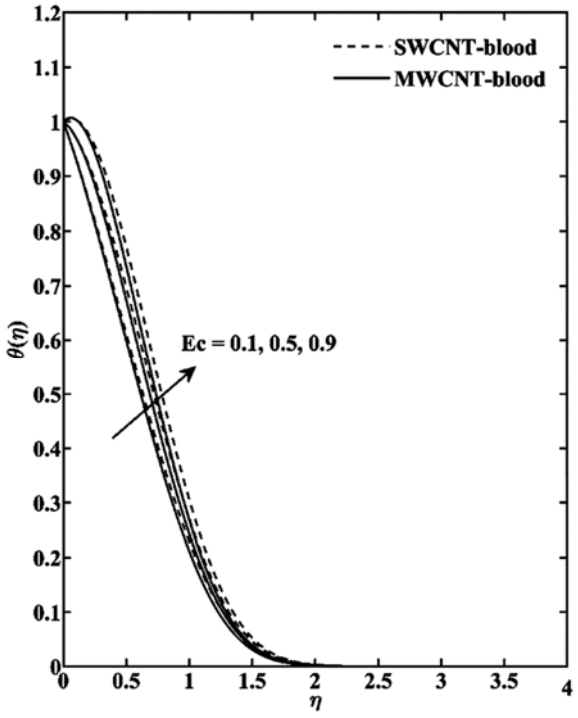


Fig. 11 — Temperature profile for Eckert number $Ec$ .

to the Eckert number $Ec$ for the SWCNT-blood and MWCNT-blood nanofluids. The velocity and temperature of the fluid increase for the rising values of Eckert number for both nanofluids. The Eckert number measures the energy conversion occurring in a flow realm. An increase in the Eckert number signifies a rise in the kinetic energy of the fluid relative to its enthalpy, which results in a rise in the flow velocity. Furthermore, the higher the Eckert number, the more energy dissipated, so the fluids' temperature increases.

It has also been observed from the figures (2) – (11) that except the velocity profile for radiation parameter and Eckert number, the velocity profile of MWCNT-blood nanofluid dominates the velocity profile of SWCNT-blood. However, the reverse trend was noticed for the temperature profiles for both nanofluids for all other governing parameters.

## 6 Conclusion

The current work explores an incompressible unsteady two-dimensional MHD flow of CNTs-blood nano-liquid flow under viscous dissipation, resistive heating, and thermal radiation. Here, the temperature-dependent viscosity has been assumed. The key outcomes noticed in the current investigation have been summarised as under

I. The local skin friction factor for the MWCNT-blood nano-liquid is superior to the SWCNT-blood nano-liquid. However, opposite results can be sighted for the local Nusselt number.

II. The velocity profile of MWCNT-blood nanofluid is higher than the velocity profile of SWCNT-blood nanofluid except for radiation parameter and Eckert number. A reverse trend has been noted for temperature profiles for both nanofluids for all other governing parameters

III. The local skin friction factor increases corresponding to the booming values of the magnetic parameter, magnetic field inclination angle, and radiation parameter for both CNTs-blood nano-liquids. At the same time, contrary results have been obtained for the unsteadiness parameter and Eckert number for both CNTs-blood nano-liquids.

IV. The local Nusselt number rises when the unsteadiness parameter, magnetic field inclination angle, and radiation parameter enhances for both CNTs-blood nano-liquids, but converse behavior can be seen for the magnetic parameter and Eckert number for both CNTs-blood nano-liquids.

V. The velocity distribution for the fluid flow enhances along with the increasing values of

the magnetic parameter, magnetic field inclination angle, radiation parameter, and Eckert number, except for the unsteadiness parameter for both CNTs-blood nano-liquids.

VI. The temperature distribution for the fluid flow reduces, corresponding to the growing values of unsteadiness, magnetic parameters, and magnetic field inclination angle for both CNTs-blood nano-liquids. However, contrary outcomes have been observed for the radiation parameter and Eckert number for both CNTs-blood nano-liquids.

**Acknowledgment**

Ajay Singh (09/964(0014)/2018-EMR-I) is grateful to CSIR, New Delhi, for financial assistance as a Senior Research Fellowship.

**References**

1 Zainal N A, Nazar R, Naganthran K & Pop I, *Int Commun Heat Mass Transf*, 134 (2022) 106020.
2 Khazayinejad M & Nourazar S S, *Int J Therm Sci*, 172 (2022) 107265.
3 Hashim, Hamid A & Khan M, *J Taiwan Inst Chem Eng*, 103 (2019) 126.
4 Biswas R, Hossain M S, Islam R, Ahmmed S F, Mishra S R & Afikuzzaman M, *J Comput Math Data Sci*, 4 (2022) 100048.
5 Raghunath K, Ganteda C, Dasore A, Kumar M L, Laxmaiah G, Hasan M A, Islam S & Razak A, *Case Stud Therm Eng*, 44 (2023) 102875.
6 Hartmann J, K Dan & Selsk V, *Mat-Fys Medd*, 15 (1937) 1.
7 Tian X Y, Li B W & Hu Z M, *Int J Heat Mass Transf*, 127 (2018) 768.
8 Chaudhary S & Kanika K M, *SN Appl Sci*, 1 (2019) 1709.
9 Patil V S, Patil A B, Ganesh S, Humane P P & Patil N S, *Mater Today Proc*, 44 (2021) 3767.
10 Doley S, Kumar A V & Lawrence J, *Compt Therm Sci*, 14 (2022) 59.
11 Alsaedi A, Muhammad K & Hayat T, *Alex Eng J*, 61 (2022) 8355.
12 Mahdy, Chamkha A J & Nabwey H A, *Alex Eng J*, 59 (2020) 1693.
13 Ali B, Hussain S, Nie Y, Hussein A K & Habib D, *Powder Technol*, 377 (2021) 439.
14 Rasool G, Ahammad N A, Ali M R, Shah N A, Wang X, Shafiq A & Wakif A, *Case Stud Therm Eng*, 42 (2023) 102654.
15 Choi S U & Eastman J A, *Proc ASME Int Mech Eng Congress Expo*, 66 (1995).
16 Krishna M V & Chamkha A J, *Res Phys*, 15 (2019) 102652.
17 Aly E H & Pop I, *Powder Technol*, 367 (2020) 192.
18 Chaudhary S, Singh A & Kanika K M, *Int J Comput Methods Eng Sci Mech*, 22 (2021) 170.
19 Maiti H, Khan A Y, Mondal S & Nandy S K, *J Comput Math Data Sci*, 6 (2023) 100074.
20 Maynes D & Webb B W, *Int J Heat Mass Transf*, 47 (2004) 987.
21 Chaudhary S & Kanika K M, *Indian J Pure Appl Phys*, 57 (2019) 861.
22 Gholinia M, Hoseini M E & Gholinia S, *Therm Sci Eng Prog*, 11 (2019) 272.
23 Khan M R, Mao S, Deebani W & Elsiddieg A M A, *Int Commun Heat Mass Transf*, 131 (2022) 105843.
24 Doley S, Alagarsamy V K, Chamkha A J, Lawrence J & Jacob A, *Numer Heat Tr B-Fund*, 84 (2023) 24.
25 Patil V S, Patil A B, Ganesh S, Humane P P & Patil N S, *Mater Today: Proc*, 44 (2021) 3767.
26 Sedki A M, *Res Mater*, 16 (2022) 100334.
27 Siddheshwar P G & Mahabaleswar U S, *Int J Non Linear Mech*, 40 (2005) 807.
28 Daniel Y S, Aziz Z A, Ismail Z & Saleh F, *J King Saud Univ Sci*, 31 (2019) 804.
29 Chaudhary S & Kanika K M, *Phys Scr*, 95 (2020) 025202.
30 Sedki A M, Abo-Dahab S M, Bouslimi J & Mahmoud K H, *Sci Prog*, 104 (2021) 1.
31 Priyadharsini M & David M G A, *J Therm Biol*, 111 (2023) 103398.
32 Akbar N S & Khan Z H, *J Mol Liq*, 232 (2017) 4717.
33 Kumar T S, *Partial Differ Equ Appl Math*, 4 (2021) 100070.
34 Tripathi D, Prakash J, Tiwari A K & Ellahi R, *Microvasc Res*, 132 (2020) 104065.